

## BIO-SYNTHESIS OF NiO AND Ni NANOPARTICLES AND THEIR CHARACTERIZATION

A. AYESHA MARIAM<sup>a\*</sup>, M. KASHIF<sup>b</sup>, S. AROKIYARAJ<sup>c</sup>,  
M. BOUOUDINA<sup>d,e</sup>, M. G. V. SANKARACHARYULU<sup>f</sup>, M.  
JAYACHANDRAN<sup>g</sup>, U. HASHIM<sup>b</sup>

<sup>a</sup>*Department of Physics, Khadir Mohideen College, Adirampattinam, 614 701, India*

<sup>b</sup>*Nano Biochip Research Group, Institute of Nano Electronic Engineering (INEE), Universiti Malaysia Perlis (UniMAP), 01000 Kangar, Perlis, Malaysia*

<sup>c</sup>*Animal Nutrition and Physiology, National Institute of Animal Science, Republic of Korea*

<sup>d</sup>*Nanotechnology Centre, University of Bahrain, PO Box 32038, Kingdom of Bahrain*

<sup>e</sup>*Department of Physics, College of Science, University of Bahrain, PO Box 32038, Kingdom of Bahrain*

<sup>f</sup>*Arignar Anna Government Arts & Science College, Karaikal, Karaikal District, 609605, India*

<sup>g</sup>*Electro Chemical Material Science Division, Central Electro Chemical Research Institute (CSIR), Karaikudi, 630 006, India*

NiO and Ni nanoparticles (NPs) were successfully synthesized by boiling method using leaves of *Azadirachta indica* and *Psidium guajava*. The size and morphology of the particles was found to be in the range of 17-77 nm by Transmission electron microscopy and Scanning electron microscopy. X-ray diffraction analysis and Atomic mass spectrograph confirms the formation of pure Ni and NiO cubic phases with an average crystallite size of 44 and 22 nm. The absorbance of NiO nanoparticles were observed by absorbance spectra and magnetic flux density values are 60 emu/g of this sample but for metallic nanoparticle of Ni there was no absorbance was observed. Further the synthesised Ni and NiO nanoparticles showed cytotoxic effect against HT29 cell line. Further study is required to identify the anticancer mechanism of the synthesised Ni and NiO nanoparticles that may use for cancer therapy.

(Received June 17, 2014; Accepted August 11, 2014)

*Keywords:* Ni and NiO; nanoparticles; SEM and TEM; magnetic properties, Cytotoxic.

### 1. Introduction

More attention has been devoted on nanoscale magnetic transition metal-based materials, including Ni, Co and Fe due to their superior magnetic properties and potential applications. Integration of green chemistry principles to nanotechnology is one of the key issues in nanoscience research. Nanobiotechnology combines biological principles with physical and chemical procedures to generate nano-sized particles with specific functions. Recently many attempts have been made to develop processes and techniques that would yield nanoparticles (NPs) with definite size and shape (Matijevic, 1993). Jennifer A. et al. (2007) reported that, the nature of engineered nanomaterials and their proposed uses provides compelling reasons for the implementation of green chemistry in the development of new materials and applications. The technology is in their early development stage and expected to be widely applied and distributed. These materials are expected to (i) exhibit new size-based properties (both beneficial and detrimental) that are

---

\*Corresponding author : aismma786@gmail.com

intermediate between molecular and particulate; (ii) incorporate a wide range of elemental and material compositions, including organics, inorganics, and hybrid structures; and (iii) possess a high degree of surface functionality.

NPs of metals and semiconductors have an immense use in various other branches of sciences. There are various chemical and physical methods to synthesize NPs, which require tedious and environmentally challenging techniques (Armstead and Li, 2011). The growing needs to develop clean, non-toxic and eco-friendly procedures for the synthesis of NPs has resulted in researchers seriously looking at biological systems for inspiration. Ever increasing pressure to develop environmentally benign technique for NPs synthesis has led to a renewed interest in biotransformation as a route for the growth of nanoscale microstructures. Biological systems have a unique ability to control the structure, phase and nano-structural topography of the inorganic crystals (Yi et al., 2001). Nickel NPs have attracted much attention because of their applications as catalysts and as magnetic materials (Kurihara et al., 1995). The usual preparation methods have been carried out by adding  $\text{NaBH}_4$  to avoid the formation of nickel oxide or hydroxide (Chen and Wu, 2000). There are several reports on the preparation of Ni NPs; nevertheless these methods use organometallic precursors (Hyeon, 2003), reverse micelles and templates (Chen and Wu, 2000; Peng, 2010). Many of the applications are size and shape dependent and thus the control of particle size is essential (Samia et al., 2006). Additionally, it has been reported that Nickel NPs have shown good antibacterial activity against *E. coli*, *L. cassie*, *S. aureus*, *P.aeruginosa* and *B. subtilis* (Chevellier, 1996).

In this study, pure and single phase NiO and Ni NPs were successfully synthesized by a simple and cost-effective boiling method using leaves of *Azadirachta indica* and *Psidium guajava*. The obtained powders were characterised by XRD, SEM and TEM, UV-vis, and magnetic measurements followed by *in vitro* cytotoxic effect against HT-29 cell lines.

## 2. Experimental Part

### Plant Collection and Extraction

*Azadirachta indica* and *Psidium guajava* leaves were collected and thoroughly washed with distilled water. The leaf broth was prepared by mixing 5gm of thoroughly washed and finely cut leaves and 15 ml of Milli Q water. Then the leaves were nicely crushed in mortar pestle, after that the nicely crushed leaves were transferred into a centrifuge tube and centrifuged (Optima L-100XP Ultra centrifuge, Rotor NU 70.1, Beckman-Coulter, USA) at a speed of 10000 -11000 rpm for 10 min at 4 to 5°C. After centrifugation, the supernatant was filtered using *Whatmann paper* and filtrate was used for the synthesis of NiO and Ni NPs.

### Synthesis of Ni and NiO nanoparticles

Seven ml of Nickel chloride solution (1% of Ni chloride  $\text{NiCl}_2 \cdot 6\text{H}_2\text{O}$ , MERCK) was mixed with the obtained biological extract and added into 25 ml of boiling Milli Q water. Within a few minutes; the solution developed a distinct characteristic color (brown-red). The particles were purified by centrifugation (Yield 0.2%), lyophilized and stored in screw capped bottles under ambient conditions for further characterization and cytotoxic studies.

### Characterisation

Phase identification and crystallite size determination were carried out using X-ray diffractometer (PANalyticalX'Pert) at  $\text{CuK}_\alpha$  radiation,  $\lambda = 1.5406 \text{ \AA}$ , using the  $2\theta$  range of 20–80° with step width of 0.02° and step time 2.40 s. TEM images and selected area electron diffraction (SAED) patterns were recorded using a 200 KV Tecnai-20 G2 TEM instrument. The surface morphology of the samples was investigated by scanning electron microscopy, SEM Hitachi S-3400N. The magnetic properties were determined with a commercial Superconducting Quantum Interference Device magnetometer (VSM-SQUID) from Quantum Design for temperatures 5–400 K and external magnetic fields up to 3 T.

### ***In-vitro* Cytotoxic activity**

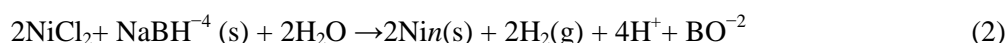
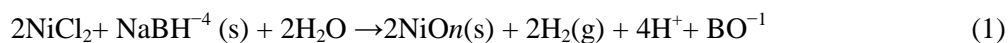
The *in vitro* cytotoxicity activity was done using HT- 29 cell line (Human colon adenocarcinoma, Lifetech Research Center, Chennai). Cells were grown in Minimal essential medium supplemented with 2 mM L- glutamine, 10% Fetal Bovine Serum, Penicillin (100 µg/ml), Streptomycin (100 µg/ml) and Amphotericin B (5 µg/ml) and maintained at 37°C in a humidified atmosphere with 5% CO<sub>2</sub> and subculture twice a week. MTT assay (3-[4,5-imethylthiazol-2-yl]-2,5 - diphenyl tetrazolium bromide) was performed to assess the cytotoxicity of the synthesised Nickel nanoparticles. The cells were cultured in 96-well microtitre plates, treated with varying concentrations of different plant extracts for 6-7 days and incubated. At the end of the treatment period, MTT was added to each well and the plates incubated for 3 h in a dark chamber. 100 µl of DMSO was added to dissolve the formazan crystals and the absorbance read at 540 nm using ELISA reader (Zhu et al., 2001). Exponentially growing cells were harvested, counted with haemocytometer and diluted with a particular medium. The diluted ranges of extracts were added to each well and the final concentrations of the test extracts were 1000, 500, 250, 125, 62.5, 31.2, 15.6 and 7.8 µg/ml. The incubation period used was 72 h. After solubilization of the purple formazan crystals were completed, the spectrophotometrical absorbance of the nickel nanoparticles produced by the plants extract was measured using an ELISA reader at a wavelength of 550 nm. The relative cell viability (%) related to the control wells that contained the cell culture medium without nanoparticles as a vehicle was calculated by

$$\% \text{ Cell Viability} = \frac{(A) \text{ Control} - (A) \text{ test}}{(A) \text{ Control}} \times 100$$

Where (A) test is the absorbance of the test sample and (A) control is the absorbance of the control sample. Non-treated cells were used as the control, and the samples were imaged using an inverted photomicroscope. The Values of MTT assay correspond to mean and standard deviations of three independent experiments.

### **3. Results and Discussion**

The formation of NiO and Ni nanoparticles was noticeable by the dramatic colour change of the product after the introduction of the reducing agent. The overall reactions proposed for the processes leading to the formation of NiO and Ni NPs could be sketched as follows:



Hydrazine is a one of the most powerful reducing agent. Temperature and time of the reaction influence the final products. Between 60 and 70°C and under basic condition, the reaction (1) proceeds fast and leads to NiO NPS and Ni NPs. The analysis of the solution remaining after the solid removal (data not shown) indicates the presence of Na<sup>+</sup>, Cl<sup>-</sup> and BO<sup>-2</sup> ions, which corroborates the proposed mechanism when it is incorporated with *A. indica* and *P. guajava* give NiO and Ni. Water was provided by the hydrated salt used as precursor (NiCl<sub>2</sub>.6H<sub>2</sub>O).

The corresponding XRD patterns for the prepared NiO and Ni nanoparticles from *A. indica* and *P. guajava* were shown in Figure 1 and the diffraction peaks were indexed according to JCPDS cards No. 45-1027 and 04-0850, respectively. The observed peaks revealed that the obtained particles are pure cubic face centred and average crystallite size were calculated to be 22 nm and 44 nm. All the diffraction peaks are in good agreement with the JCPDS (45-1027) data showing that the main structure of the sample is cubic NiO NPs and JCPDS (04-0850) data showing that the main structure of the sample 2 is Ni. The Full Width Half Maximum (FWHM) of NPs shows a decreasing trend with different planes of NiO and Ni NPs. From the crystallite size the dislocation density value was calculated by the formula [4];

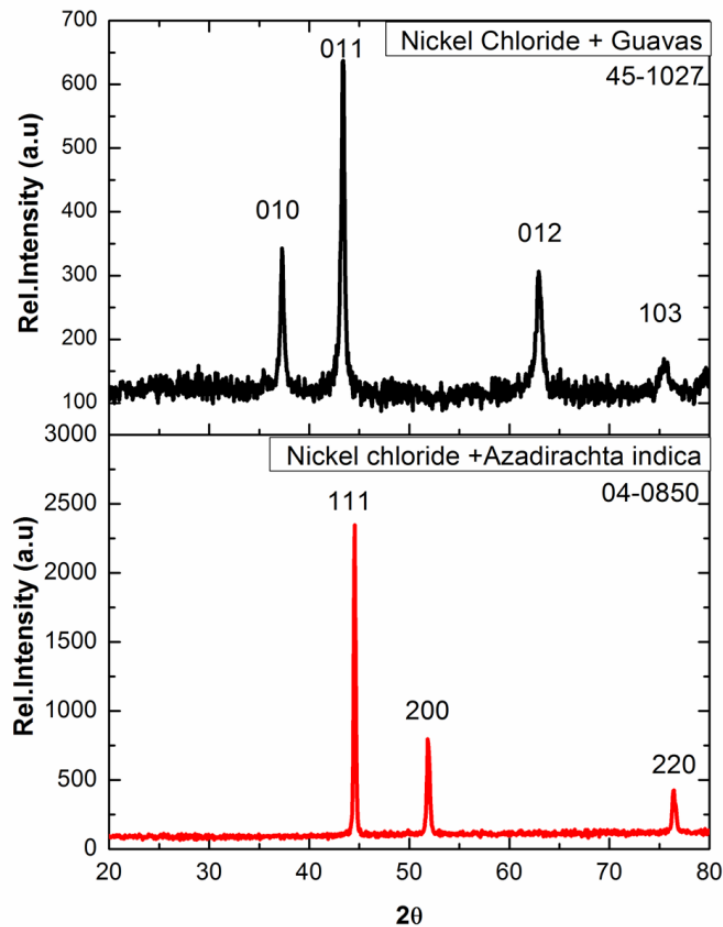


Fig. 1. XRD patterns of biosynthesised NPs using leaves (a) NiO by Guavas leaves and (b) Ni by Azadirachta indica.

Dislocations are imperfection in a crystal associated with the misregistry of the lattice in one part of the crystal with that in another part. Unlike vacancies and interstitial atoms, dislocations are not equilibrium imperfections (i.e.) thermodynamic considerations are insufficient to account for their existence in the observed densities. In the present study, the dislocation density is estimated from the relation:

$$\frac{1}{D^2} \text{ lines/m}^2. \quad (4)$$

The measured line-widths and the other physical parameters are calculated and are given in Table 1. From the Table 1, it can be concluded that the crystallite size increases for the different planes.

The crystallite size of the as-prepared powders is estimated using Scherer formula:

$$D = \frac{0.94 \lambda}{\beta \cos \theta} \quad (5)$$

where  $\lambda$  is the wavelength of the incident beam ( $\lambda_{\text{Cu}}=1.5406 \text{ \AA}$ ) and  $\beta$  the full width at half its maximum,  $\theta$  is the Bragg's diffraction. The width of XRD lines is determined by statistical contribution based on a combination of microstrain and crystallite size. The two effects can be separated when higher order reflections are present. The statistical microstrain:

$$\varepsilon = \frac{\Delta d}{d_o} = \frac{\Delta d}{d_{hkl}} \quad (6)$$

From Rietveld analysis we observed that NiO NPs are 30 nm and Ni NPs are having diameter 103 nm lattice parameter for NiO are 4.1690 Å and for Ni are 3.5246 Å and micro strain values are also well matched with structural studies when it was compared with Table 1 and Table 2.

Table 1. Refinements results as obtained by the Rietveld method: phase composition, microstructural parameters (crystallite size and microstrain), and fit parameters.

Morphology	Miller indices (hkl)	Interplanar distance (Å)	Grain Size (Å)	Lattice constants (a and c)	Strain $\text{line}^{-2}\text{m}^{-4}$	Dislocation density $= \frac{1}{D^2} \times 10^{15}$ lines/m <sup>2</sup>
Sample 1 (NiO)	010	2.3018	28.25	a = 4.157 Å	-0.0453	1.253
	100	2.0334	31.55	V = 71.84 Å <sup>3</sup>	-0.02535	1.005
	012	1.5784	18.36		0.06957	2.966
	103	1.2239	8.335	-0.0270	14.30	
Sample 2 (Ni)	111	2.03387	56.45	a = 3.5226 Å	0.000064	3.138
	200	1.76165	33.84	V = 43.71 Å <sup>3</sup>	0.000199	8.732
	220	1.24567	42.95	0.000246	5.421	

Table 2. Structural parameters of sample 1 (NiO) and Ni for and sample 2 (Ni) NPs

Sample	Phase	Crystallite size (nm)	Microstrain $\times 10^{-3}$ line/m	Lattice parameter a (Å)	Fit parameters
Sample-1	NiO	30	0.480	4.1690 (19)	$R_{wp}=9.30$ $R_e=7.34$ $R_p=8.90$ $S=1.04$ $\chi^2=1.09$
Sample-2	Ni	103	0.191	3.5246 (4)	$R_{wp}=9.13$ $R_e=7.13$ $R_p=9.26$ $S=0.98$ $\chi^2=0.97$

The diffraction peaks are corresponding to typical face centered cubic structure of NiO and Ni NPs has been structured with phase of Fm-3m (225). No indication of oxide or impurity phases is observed by Atomic Mass Spectrograph. The crystallite size of Rietveld refinement parameter for the NPs was calculated and tabulated in Table 2, diffraction peak corresponding to the Bragg's angle. The calculated mean crystallite sizes of XRD of the NiO and Ni NPs is 30 and 103 nm. Note that the value agrees to that determined from the HRTEM images of XRD tabulated in Table 1.

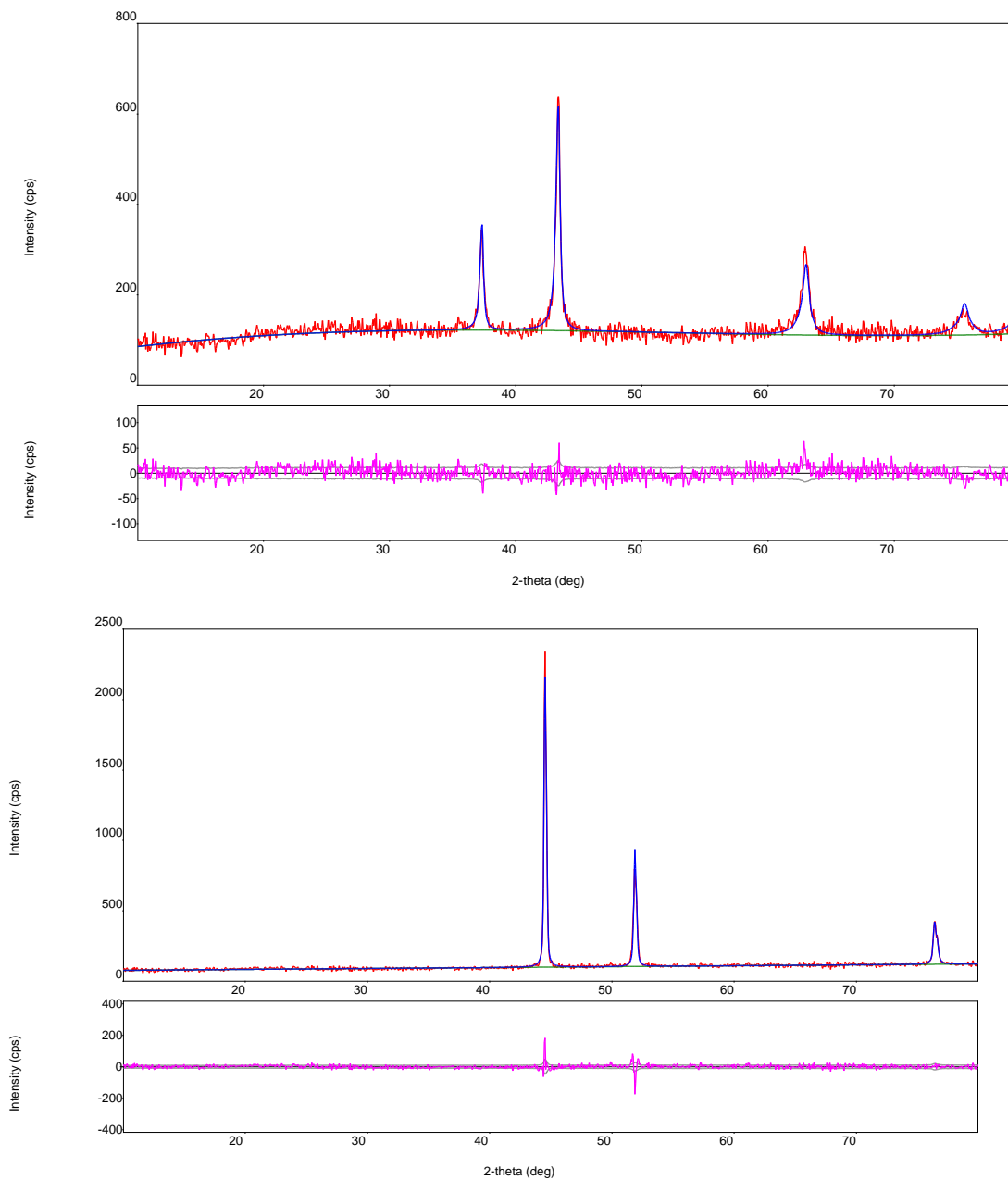


Fig. 2. Rietveld Analysis of XRD pattern of as-prepared NiO and Ni NPs (dots: experimental intensity, upper solid line: calculated intensity, lower solid line: the intensity difference).

The morphology of NiO/Ni NPs shown in Figure 3 indicates that the particles are less than 100 nm and in spherical shapes. The appearance of some darker particles results from an enhanced diffraction contrast due to their orientation with respect to the electron beam. All the particles showed a narrow particle size distribution. Due to the large surface to volume ratio and strong magnetic attraction forces, the NiO/Ni NPs tend to agglomerate in order to minimize the total surface energy of the system. The selected-area electron diffraction (SAED) patterns in the inset reveal that the samples are crystalline or semi crystalline.

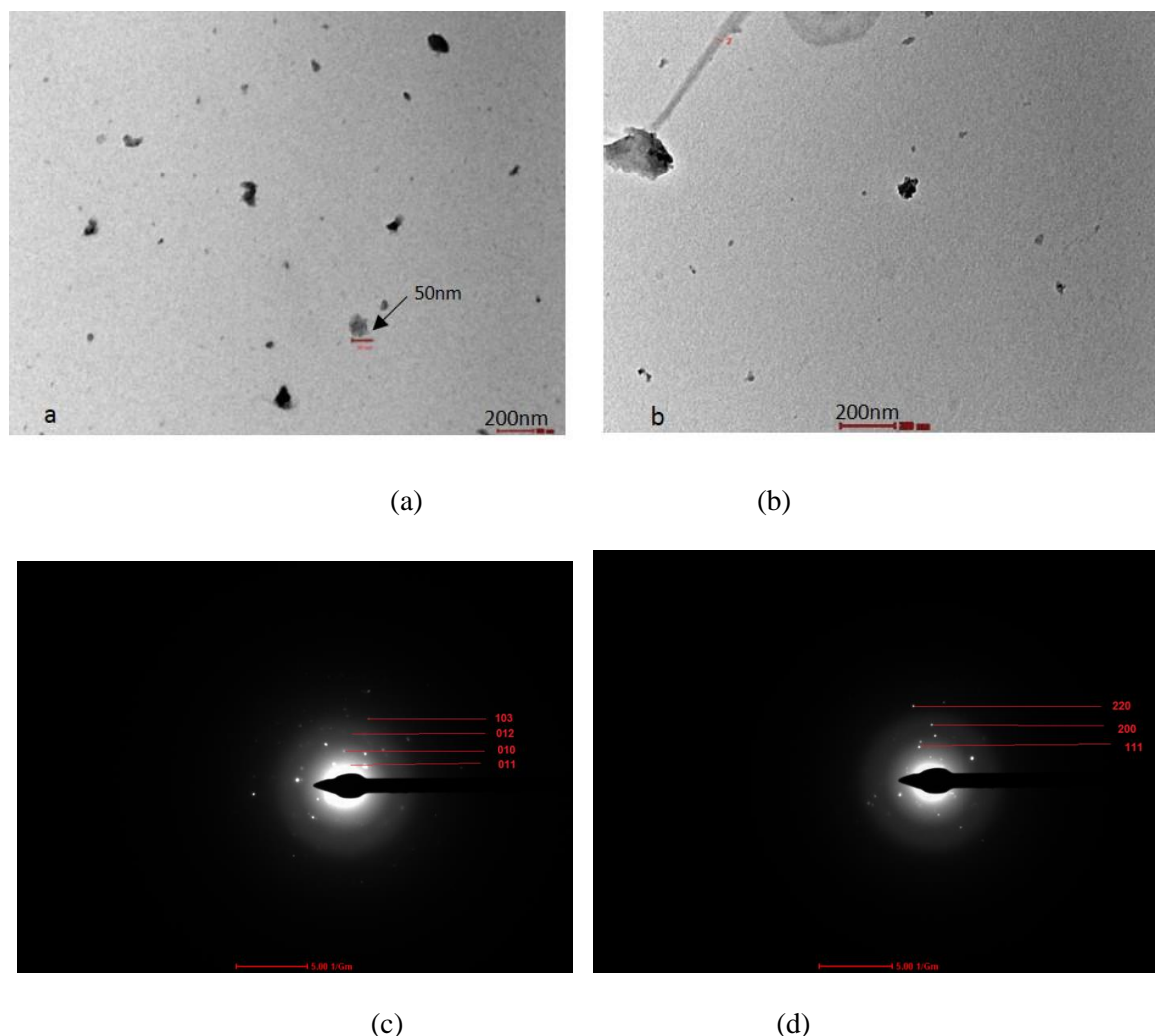


Fig. 3. TEM analysis biosynthesized NPs using extract of leaves (a) NiO by Guavas, (b) Ni NPs by Azadirachtaindica, (c) SAED of NiO, and (d) SAED Ni.

The morphology of the samples was investigated by field emission scanning electron microscopy (Figure 4a,b). The particles are found to be spherical in the size range between 17 – 70 nm, aggregation due to bioactive compounds present in *A. indica* and *P. guajava*. The size of the produced NPs are in the nanoscale range depending on the molar ratio of  $(\text{NiCl}_2 \cdot 6\text{H}_2\text{O})$  between 0.5 to 1. There is no optical properties of Ni metal NPs and NiO NPs are having the absorbance value 0.2 to 0.8 Å proved that the band gap values at 327 nm. In the present work, the optical band gap is calculated using the Tauc relation as described by the following expression [13]:

$$(\alpha h\nu)^{1/n} = A(h\nu - E_g)$$

where  $A$  is a constant and  $E_g$  is the band gap of the material and exponent  $n$  depends on the type of transition. For direct allowed transition  $n=1/2$ , indirect allowed transition  $n=2$ , direct forbidden transition  $n=3/2$  and forbidden indirect transition  $n=3$ . To determine the possible transitions,  $(\alpha h\nu)^2$  vs  $h\nu$  curve is plotted and the corresponding band gap can be obtained from extrapolating the straight portion of the graph on  $h\nu$  axis. The direct band gap values of the samples have been obtained from  $(\alpha h\nu)^2$  vs plot are shown in the Figure 5c. The direct band gap value for NiO is found to be 2.69 eV.

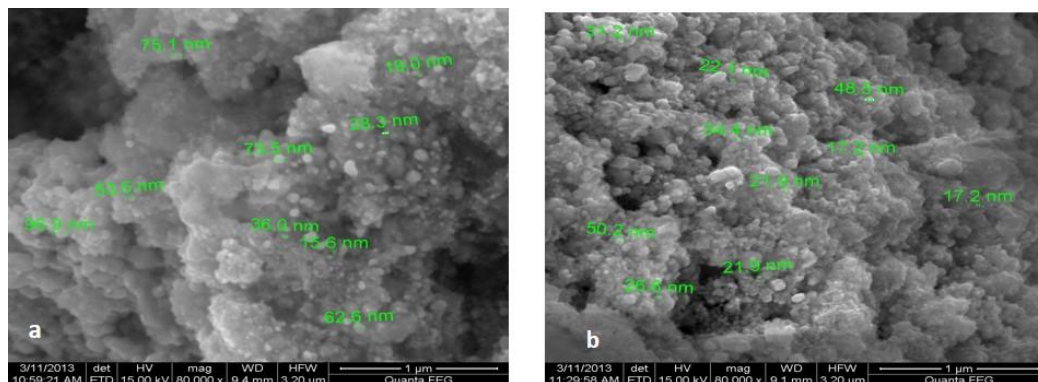


Fig. 4. SEM analysis of biosynthesized NPs using leaves (a) NiO by Guavas and (b) Ni by Azadirachta indica.

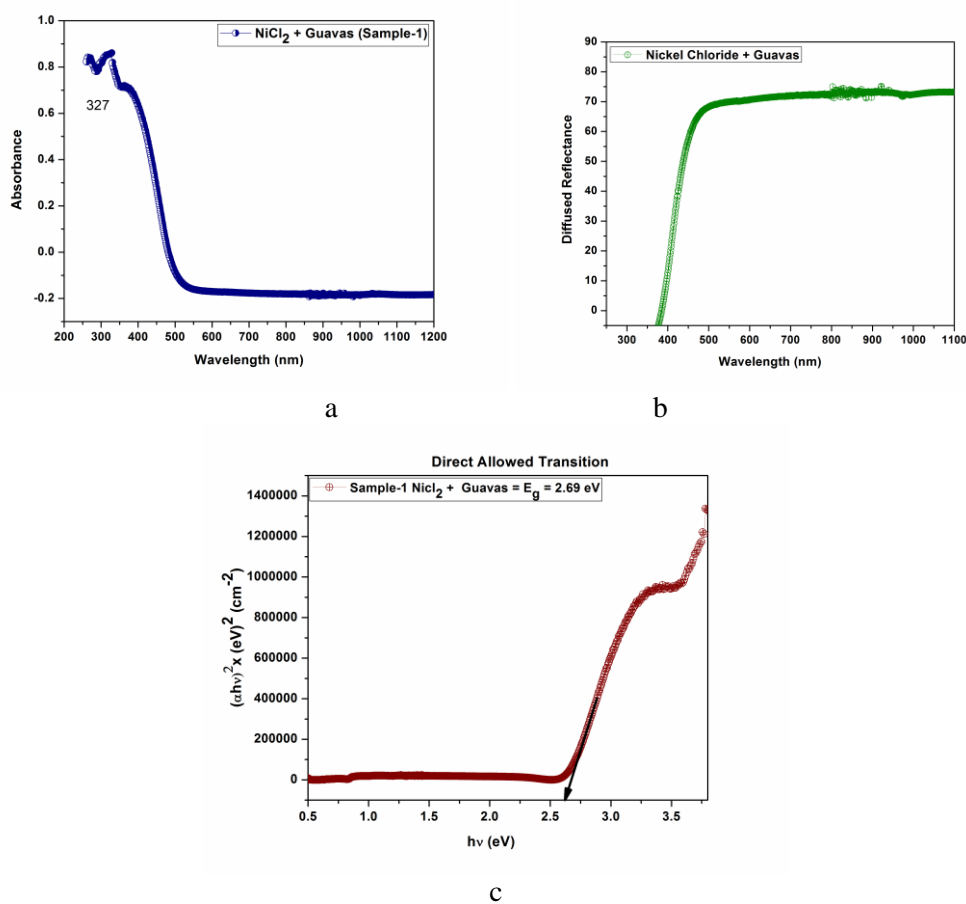


Fig. 5. UV-vis, (a) absorbance, (b) diffusive reflectance and (c) Tauc plot

Magnetisation-Field (M-H) hysteresis loops of NiO/Ni NPs (Figure 6) reveal a room temperature ferromagnetism (RTF). The hysteresis loop of the NiO NPs and Ni NPs spheres under a static magnetic field (up to 3 T) at room temperature revealed the paramagnetic behavior of the material. We measured a saturation magnetization  $M_s$  of 63 emu/g and 40 emu/g. The zero coercivity characteristic of the NiO NPs and Ni NPs spheres implies that the Ni NPs size is less than a critical value at which the magnetic effects become strong enough to spontaneously demagnetize a previously saturated assembly of particles (Ibrahim et al., 2012; Ibrahim et al., 2012). Therefore, the coercivity drop to zero and the particles behave like paramagnetic systems.

Noteworthy, the paramagnetic composites are highly desired for biological applications due to their well dispersion in solutions.

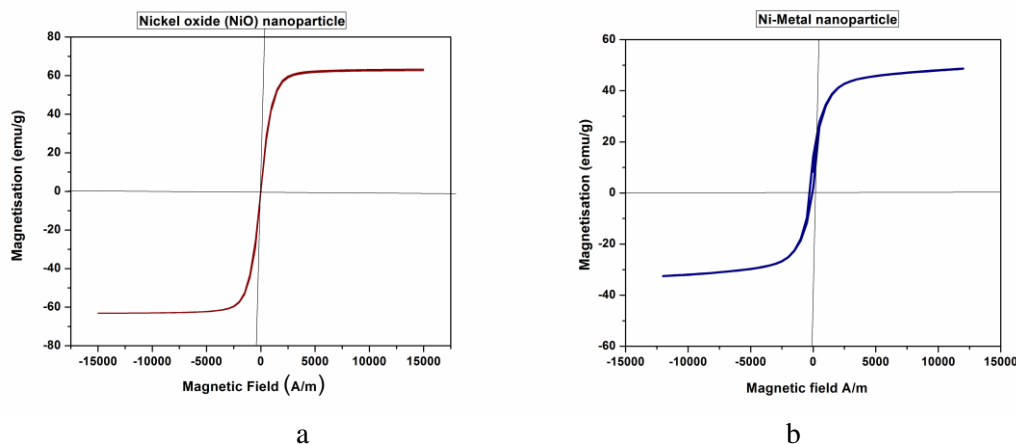


Fig. 6. *M-H* hysteresis loops measured at room temperature of Biosynthesised NPs (a) NiO NPs by (Guavas) Koyya and (b) Ni by Neem (*Azadirachta indica*)

After the extrapolation of the magnetization, the saturation magnetization was estimated to be 60 emu/g, which also supports the conclusion that nearly all hydroxide precursors is converted into nickel oxide. The Ni nano powder synthesised by using *A. indica* and *P. guajava* are shown in Figure 4. The magnetization increases slightly from 39.92 emu/g for sample 2 biosynthesised by Guavas (Auffan et al., 2009) and for the sample 2 magnetization increases to 63 emu/g bio synthesised by *A. indica*, this increase may be associated with the structural perfections of sample 2 than sample 1. This increase in magnetization is possibly attributed to a shift in the nickel concentration during biosynthesis. The pure NiO possesses a saturation magnetization of 39.92 emu/g for sample 1, while the nickel has a magnetization of 63 emu/g for sample 2.

NiO is a good magnetic material nearly for bulk 60 emu/g, with magnetic saturation ( $M_s$ ) moments of 63 emu/g for sample 1, and magnetic saturation ( $M_s$ ) moments 61 emu/g of sample 2 Ni nano particles these values are found to be smaller for the corresponding particles, which has been attributed to the surface effects, these values are close to the bulk Ni particles. Ni nanoparticles sizes ranging from 17-70 nm represent an important class of artificial nanomaterials. At this scale regime, the thermal energy is sufficient to overcome the anisotropy energy, therefore the magnetic moment begin to fluctuate randomly. More specifically, the relaxation of the magnetisation orientation of each particle is determined by

$$\tau = \tau_0 e^{Kv/2kt}$$

where  $\tau$  is the relaxation time at one orientation,  $K$  is the particle's anisotropy constant,  $V$  is the particle volume,  $k$  is the Boltzmann's constant, and  $T$  is the temperature. As the size of the particle decreases to a level where  $KV$  (free-energy barriers), becomes comparable to  $kT$  (thermal energy), its magnetization starts to fluctuate from one orientation to another, leaving no coercivity and net magnetic moment (Gu et al., 2004; Teranishi et al., 2004).

Table 3. Atomic mass spectroscopy of sample 1 (NiO) and Ni for and sample 2 (Ni) NPs

S.No	NAME OF THE PARAMETER	SAMPLE DETAILS	
		NiO	Ni
<b>PHYSICAL PARAMETER</b>			
1.	Electrical conductivity ( $\text{dsm}^{-1}$ )	0.46	0.45
<b>ANIONS</b>			
2	Carbonate (mg/l)	Nil	Nil
3	Bi Carbonate (mg/l)	2.7	2.6
4	Chloride (mg/l)	12.0	13.6
5	Sulphate (mg/l)	0.56	0.59
6	Phosphate (mg/l)	0.23	0.22
7	Nitrate (mg/l)	0.06	0.05
8	Fluoride (mg/l)	0.03	0.02
<b>CATIONS</b>			
9	Calcium (mg/l)	43	42
10	Magnesium (mg/l)	34	36
11	Sodium (mg/l)	33	30
12	Potassium (mg/l)	0.04	0.05
<b>HEAVY METALS</b>			
13	Nickel (Neem)(mg/l)	0.03	--
14	Nickel oxide (Koyya) (mg/l)	--	0.02

Figures 4a and 4b show the simulated hysteresis loops for a nickel bio synthesized nanoparticles under different a reducing agents of *A. indica* and *P. guajava* leaves, it increase the levels of tensile and compressive stress. The hysteresis loops displayed systematic changes under different products of bio leaves. Table 3 shows the variations of coercivity, applied magnetic field, mass and retentivity with different reducing agent. The results show that the coercivity increased significantly with increasing compressive stress and decreased slightly with increasing tensile stress. The modeling results are in good qualitative agreement with the experimental data on nickel nanoparticle found in the literature (Auffan et al., 2009) but are quite different from those reported on bulk nickel samples (Jiles et al., 1988). Such differences can be attributed to the different effects of biosynthesized extracts on two different mechanisms of magnetization reversal, namely, irreversible domain rotation and domain wall movement (Garshelis, 1993). It has been pointed out that when the reversal process is dominated by irreversible domain rotation, the field required to switch the domain magnetization. Will increase if the easy axis induced by the external stress is parallel to the biosynthesis extracts e.g., compressive stress applied to nickel along the field direction (Callegaro and Pupin, 1996). This can be explained by considering the coherent rotation of domain magnetization against the stress-induced uniaxial anisotropy under a different extract. As described by other anisotropic models, such as the Stoner–Wolfarth model, the critical field at which the domain magnetization switches abruptly increases with the anisotropy. Therefore it was expected that the coercivity of the model system, for which the magnetization reversal process involved is essentially irreversible rotation of magnetic moments, would increase with increasing compressive stress along the field direction. Similarly the coercivity was expected to decrease when the easy axis induced by the external stress was perpendicular to the two different reducing agents of bio leaves e.g., tensile stress on nickel along the field direction.

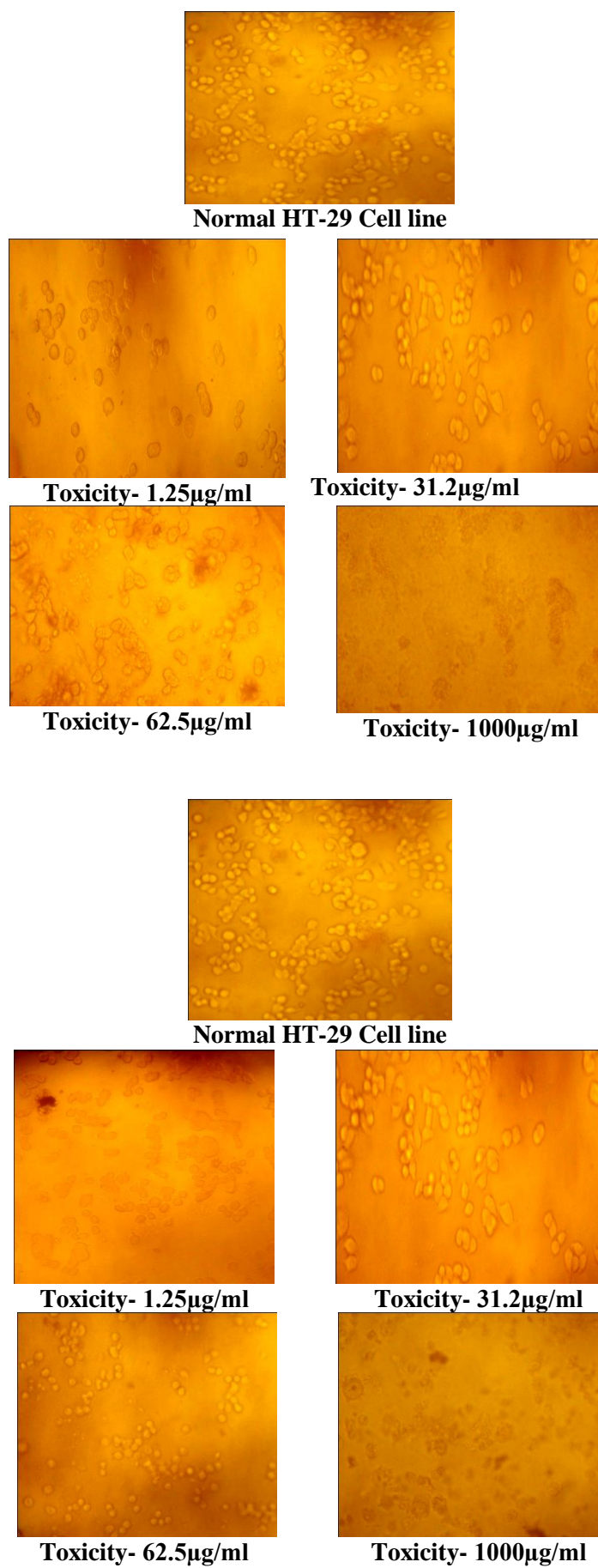


Fig. 7 Morphological observation of HT-29 Cell line treated with NiO and Ni NPs

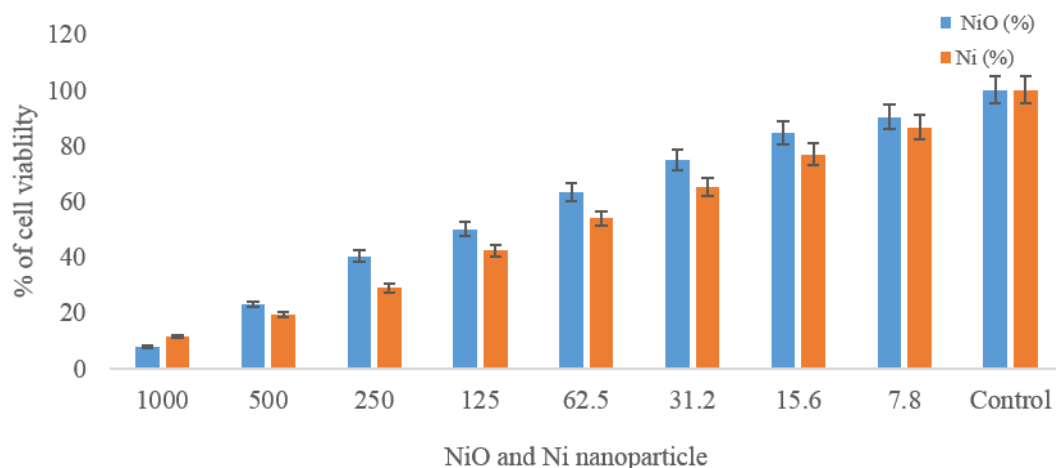


Fig. 8. Evaluation of cell concentration and cell viability of NiO and Ni NPs

Table 4. Magnetic properties of for sample 1 (NiO) and sample 2 (Ni) NPs

Sample	NiO	Ni
Coercivity (Hci), G	17.79	6.7907
Saturation Magnetization (Ms), emu/g	39.622	63.218
Remanence (Mr), emu/g	0.4656	0.35178
Mass, g	0.256	0.17389

In this present study Nickel nanoparticles synthesised by *Azadirachta indica* and *Psidium guajava* -2 were further evaluated for the cytotoxic activity using HT-29 colon cancer cell lines (Roy et al., 2007). The % of viability of the cells in each dose was measured by using MTT assay method. The absorbance is directly proportional to the number of living cells in the culture. The observed result revealed, the cells treated with NiO and Ni nanoparticles showed significant cytotoxicity in cell lines at the concentration above 62.5  $\mu\text{g/ml}$  (Figure 8). Morphological observation of HT29 cells, showed significant changes in the cell morphology (Swelling of cells, Cell breakage) when treated with the synthesised NiO and Ni nanoparticles. Whereas, the control cell showed a regular and smooth surface with normal morphology in control cells of HT29 (Figure 7 a & b). From the above finding, we suggest further cytotoxic study to determine the anticancer mechanism by the synthesised Ni and NiO NPs.

#### 4. Conclusions

Ni and NiO nanoparticles were biosynthesised using leaves of *A. indica* and *P. guajava*. Average crystallite size of the crystals is 22 and 44 nm. The lattice constant of the Ni nanoparticles is larger than the bulk value. TEM and SEM analysis reveals that the nanoparticles were spherical in shape and toxic effect were observed in HT29 cell lines.

#### References

- [1] A.L. Armstead, B., Li, Inter J. of Nanomed. **6**, 3281 (2011)
- [2] M. Auffan, J., Rose, M.R., Wiesner, J.Y., Bottero, Environ pollut. **157**, 1127 (2009).
- [3] L. Callegaro, E. Puppini, Appl. Phys. Lett. **68**, 1279 (1996)
- [4] D.H., Chen, Wu, S.H., Chem mater. **12**, 1354 (2000).
- [5] A., Cheveller, . The Encyclopedia of Medical Plant. London. Dorling Kindersley Ltd.

- (online). [http:// www.chclibrary.org/plant.html](http://www.chclibrary.org/plant.html), 1996
- [6] I.J. Garshelis, J. Appl. Phys. **73**, 5629 (1993)
- [7] H.W. Gu, R.K., Zheng, X.X., Zhang, B., Xu, Journal of the American Chemical Society. **126**, 5664 (2004).
- [8] T., Hyeon, Synthesis of Cu<sub>2</sub>O coated Cu nanoparticles and their successful applications to Ullmann-type amination coupling reactions of aryl chlorides. Chem Commun. 927, 2003.
- [9] E.M.M., Ibrahim, S., Hampel, J., Thomas, D., Haase, A.U.B., Wolter, V.O., Khavrus, J Nanopart Res. **12**,1118 (2012).
- [10] E.M.M., Ibrahim, S., Hampel, A.U.B., Wolter, M., Kath, A.A., Gendy, R., Klingeler, J Phy Chem C.**116**, 22509 (2012).
- [11] A.D., Jennifer, L.S., Bettye, Maddux, James, E., Hutchison, Chem. Rev. **107**(6), 2228 (2007)
- [12] L.K., Kurihara, G.M., Chow, P.E., Schoen, Nanostructure Mater. **5**, 607 (1995).
- [13] E., Matijevic. Chem. Mater. **5**, 412 (1993)
- [14] G.Y. Peng, J. Li, Y. Ting, W. Zhou, L. Lidong, L. Guo, S. Yang, Phys. Chem. Chem. Phys. **12**, 10781 (2010).
- [15] M.K., Roy, M., Kobori, M., Takenaka, K., Nakahara, H., Shinmoto, S., Isobe, T., Tsushida, Phytotherapy Res. **21**(3): 243 (2007).
- [16] A.C.S., Samia, J.A., Schlueter Jiang, J.S., Bader, S.D., Qin, C.J & Lin, X.M., Chem Mater, **18**, 5203 (2006).
- [17] E.C. Stoner, E.P. Wohlfarth, Philos., Trans. R. Soc. London, Ser. A **240**, 599 (1948)
- [18] T. Teranishi, Y. Inoue, M. Nakaya, Y. Oumi, T. Sano, Journal of the American Chemical Society. **126**, 9914 (2004)
- [19] D. C. Jiles, T.T. Chang, D.R. Hougen, R. Ranjan, J. Appl. Phys. **64**, 3620 (1998)
- [20] C., Yi, J., Lincoln, Lauhon, Mark, S., Wang, G.J., Charles, M., Lieber, Appl. Phys. Lett. **78**, 2214 (2001).
- [21] Z.A., Zakaria, Iran. J. Pharmacol. Ther. **6**, 87 (2007b).
- [22] B. Zhu, C.C.H., Lo, S.J., Lee, D.C., Jiles, J. Appl. Phys. **89**, 7009 (2001).